# Analysis of Angular Parameters of Dense Multipath Components in an Urban Macro-Cell Scenario

Martin Käske*, Reiner S. Thomä*
*Ilmenau University of Technology, Germany
Institute of Information Technology
martin.kaeske@tu-ilmenau.de

***Abstract*—In this paper we investigate the angular properties of the Dense Multipath Components (DMC) using realistic measurement data. We introduce a Gauss-Newton (GN) based algorithm to jointly estimate the parameters of the angular model that is comprised of a Von-Mises-Distribution (VMD) and an additional Uniform-Distribution (UD). We observe that the power of the DMC is in the average only one tenth of the power of the resolvable specular paths. Furthermore, we show that the DMC appear to be uniformly distributed in the angular domain in a lot of cases. This is mainly caused by a limite dynamic range of the data preventing a proper estimation of the VMD.**

## I. Introduction

The characterization of the spatial properties of a mobile radio channel plays a crucial role when channel models are to be derived or verified. A widely used approach is to use high resolution parameter estimation to decompose the measured channel into a sum of plane waves each associated with a certain Angle-of-Arrival (AoA), Angle-of-Departure (AoD), Time-of-Arrival (ToA) and complex path weights. However, it is known that this approach is not suitable in describing diffuse scattering or otherwise dense multipath components. This is mainly caused by the finite resolution of the estimator making it impossible to estimate the parameters of the huge number of propagation paths caused by diffuse scattering. Therefore, the data model has to be extended to describe diffuse scattering different from the sum of discrete paths. A model for the frequency-/delay-domain was already introduced by Richter in [1]. In [2] an joint estimator for the delay and angular parameters is presented that is based on estimating the covariance matrix of the DMC. The estimator is verified using simulation data. In [3] the angular properties are analyzed using beamforming of measurment data. The determination of the parameters of the VMD are done by visual inspection. In [4] a cluster-based approach is used to where each cluster of the specular paths is assigned a DMC-cluster. Unfortunately, details of the functioning of estimator for the angular parameters is not given. The authors present results using measurement data in an indoor scenario. In this contribution we extend the approach described in [5] by implementing a GN-algorithm for the estimation and show the results for an urban macro-cell measurement campaign.

## II. Radio Channel Data Model

The data model for the mobile radio channel used in the paper on hand is the hybrid model introduced in [1]. It is composed of a deterministic and a stochastic part. For the paper on hand we used the RIMAX-algorithm also introduced in [1] to extract the parameters of the data model from measurement data. The deterministic part accounts for resolvable specular propagation paths. It assumes plane waves and a flat frequency response of the scatterers (narrowband-assumption). Each paths is described using its ToA,AoA (azimuth $\varphi$ and elevation $\vartheta$),AoD and complex polarimetric path weight:

$$\boldsymbol{\theta}_{sp,k} = [\tau_k, \varphi_{Rx,k}, \vartheta_{Rx,k}, \varphi_{Tx,k}, \vartheta_{Tx,k}, \tag{1}$$

$$\gamma_{\varphi\varphi,k}, \gamma_{\varphi\vartheta,k}, \gamma_{\vartheta\varphi,k}, \gamma_{\vartheta\vartheta,k}] \tag{2}$$

The indices $\varphi$ and $\vartheta$ of the pathweight $\gamma$ denote the $\varphi$- and $\vartheta$-polarization respectively. The stochastic part of the data model is basically used to characterize all parts of the channel that cannot be resolved as a specular path by the estimator. This part was originally introduced to account for paths that are to closely spaced for the estimator to resolve them, hence the name "Dense-Multipath-Components". However, Landmann showed in [6] another cause for DMC namely estimation artifacts caused by imperfections of the calibration data used.

The DMC are described by its covariance matrix $\mathbf{R}$ that is assumed to be decomposible into the Kronecker-product of three matrices:

$$\mathbf{R} = \mathbf{R}_{Rx} \otimes \mathbf{R}_f \otimes \mathbf{R}_{Tx} \tag{3}$$

with $\mathbf{R}_f$ being the covariance matrix in the frequency domain and with $\mathbf{R}_{Rx}$ and $\mathbf{R}_{Tx}$ being the covariance matrix of the antenna array elements at the receiver and transmitter respectively. In [1] only a parametric model of $\mathbf{R}_f$ is given; the spatial properties of the DMC are not considered (covariance matrices set to be identity matrices). The covariance function of the DMC in the frequency-domain and the related Power-Delay-Profile (PDP) are given by:

$$\Psi_H(\Delta f) = \frac{\alpha_1}{B_d + j2\pi\Delta f} \cdot e^{-j2\pi\Delta f \tau_d} \tag{4}$$

$$\psi_h(\tau) = \begin{cases} 0 & \tau < \tau_d \\ \alpha_1 \cdot \frac{1}{2} & \tau = \tau_d \\ \alpha_1 \cdot e^{-B_d(\tau-\tau_d)} & \tau > \tau_d \end{cases} \tag{5}$$

with the parameters $\boldsymbol{\theta}_{dmc} = [\alpha_1, B_d, \tau_d]$ being the maximum value of the PDP, the coherence bandwidth and the base delay respectively.

The total data model of the radio channel is then the sum of the specular paths and the DMC. Furthermore, the additive noise $\mathbf{n}$ of the measurement device has to be accounted for:

$$\begin{aligned}\tilde{\boldsymbol{x}} &= \boldsymbol{s}\left(\boldsymbol{\theta}_{sp}\right) + \boldsymbol{d}\left(\boldsymbol{\theta}_{dmc}\right) + \mathbf{n} \\ \tilde{\boldsymbol{x}} &\in \mathcal{C}^{M_{Rx}\cdot M_{Tx}\cdot M_f \times 1}\end{aligned} \tag{6}$$

## III. Angular Data Model

Since we are interested in the characteristics of the DMC we use RIMAX [1] to estimate the specular paths and subsequently remove them from the measurement data. The spatial properties of the estimated DMC are then analyzed using beamforming to obtain an estimate for the Power-Angular-Profile (PAP). The output of the beamformer will be calculated for both polarizations and only the mean-azimuth beamformer will be used due to resolution limits of the antenna arrays used [5]:

$$\begin{aligned}A_p\left(\varphi,\vartheta\right) &= \frac{\left|\mathbf{b}_p^H\left(\varphi,\vartheta\right)\tilde{\mathbf{X}}\right|_F^2}{\left|\mathbf{b}_p\left(\varphi,\vartheta\right)\right|_F^2} \\ \tilde{\mathbf{X}} &\in \mathcal{C}^{M_{Rx}\times M_{Tx}M_f}\end{aligned} \tag{7}$$

$$A_p\left(\varphi\right) = \sum_{i=1}^{N_\vartheta} A_p\left(\varphi,\vartheta_i\right) \tag{8}$$

$\mathbf{b}_p\left(\varphi,\vartheta\right)$ denotes the steering vector of the antenna array for the $p=\varphi$- and $p=\vartheta$-polarization respectively. $\tilde{\mathbf{X}}$ denotes a reshaped matrix of the observation vector such that its dimensions suit the dimensions of $\mathbf{b}_p\left(\varphi,\vartheta\right)$. $\left(.\right)^H$ denotes complex conjugate transpose. Thereafter, we fit the curve of the beamforming output with a modified VMD and an additional UD. The Probability-Density-Function (PDF) of the VMD is given by:

$$f\left(\varphi,\mu,\kappa\right) = \frac{1}{2\pi I_0\left(\kappa\right)} e^{\kappa\cos(\varphi-\mu)} \tag{9}$$

The modification of the VMD that we apply is that its maximum value is normalized such that it matches the maximum value of the beamformer output:

$$\begin{aligned}f_m\left(\varphi,\mu,\kappa\right) &= \frac{f\left(\varphi,\mu,\kappa\right)}{f\left(\mu,\mu,\kappa\right)}\widehat{A} \\ &= e^{\kappa\cos(\varphi-\mu)}e^{-\kappa}\widehat{A}\end{aligned} \tag{10}$$

with $\widehat{A}$ being the maximum value of the beamformer output. Furthermore, an additional UD with magnitude $\alpha$ is introduced as described in [5]:

$$f_{m,UD}\left(\varphi,\mu,\kappa,\alpha\right) = e^{\kappa\cos(\varphi-\mu)}e^{-\kappa}\left(\widehat{A}-\alpha\right)+\alpha \tag{11}$$

## IV. Estimation of Angular Parameters

In order to find the adequate parameters $\mu,\kappa,\alpha$ the following optimization criterion is used:

$$\left[\widehat{\mu},\widehat{\kappa},\widehat{\alpha}\right] = \min_{\mu,\kappa,\alpha} \left|\left|A\left(\varphi\right) - f_{m,UD}\left(\varphi,\mu,\kappa,\alpha\right)\right|\right|_F^2 \tag{12}$$

We apply a GN [7] based search procedure to find the optimal values.

The GN-algorithm is an iterative optimization algorithm that can be used if the score-function is nonlinear and can be formulated as the sum of squares:

$$\begin{aligned}\epsilon\left(\boldsymbol{\theta}\right) &= \sum_{i=1}^{M}\left|\mathrm{r}_i\left(\boldsymbol{\theta}\right)\right|^2 \\ &= \mathbf{r}\left(\boldsymbol{\theta}\right)^T\mathbf{r}\left(\boldsymbol{\theta}\right) \\ \mathbf{r}\left(\boldsymbol{\theta}\right) &= \left[\mathrm{r}_1\left(\boldsymbol{\theta}\right),...,\mathrm{r}_\mathrm{M}\left(\boldsymbol{\theta}\right)\right]^\mathrm{T}\end{aligned} \tag{13}$$

With $\boldsymbol{\theta}$ being the vector of parameters whose optimal values are to be found and $\left(.\right)^T$ denoting transpose of a vector/matrix. In our case the score-function is Eqn. (12) and $\boldsymbol{\theta}=[\mu,\kappa,\alpha,]$. In order to find the optimal value the GN-algorithm uses the following update equation for the parameter vector:

$$\boldsymbol{\theta}^{n+1} = \boldsymbol{\theta}^n + \lambda^n\boldsymbol{\Delta\theta}^n \tag{14}$$

$\boldsymbol{\Delta\theta}^n$ can be interpreted as the direction in which the parameter update will take place and $\lambda^n$ as the length of the update. The update direction is computed as follows:

$$\boldsymbol{\Delta\theta} = -\left(\mathbf{J}^T\mathbf{J}\right)^{-1}\mathbf{J}^T\mathbf{r} \tag{15}$$

with $\left(.\right)^{-1}$ denoting the inverse of a matrix and $\mathbf{J}$ being the Jacobian-matrix containing the first partial derivatives of $r_i$ with respect to $\boldsymbol{\theta}$:

$$\mathbf{J} = \begin{bmatrix} \frac{\partial r_1}{\partial\theta_1} & \frac{\partial r_1}{\partial\theta_2} & \cdots & \frac{\partial r_1}{\partial\theta_N} \\ \vdots & & & \\ \frac{\partial r_M}{\partial\theta_1} & \frac{\partial r_M}{\partial\theta_2} & \cdots & \frac{\partial r_M}{\partial\theta_N} \end{bmatrix} \tag{16}$$

The parameter $\mu$ of the VMD will not be estimated by the GN-algorithm but will be set to the angle corresponding to the maximum of the beamformer $A\left(\varphi\right)$ [5]. Therefore, the parameter vector $\boldsymbol{\theta}$ will contain only the two parameters $[\alpha,\kappa]$. The individual error terms $r_i\left(\boldsymbol{\theta}\right)$ will be computed as:

$$r_i\left(\boldsymbol{\theta}\right) = A\left(\varphi_i\right) - f_{m,UD}\left(\varphi_i,\mu,\kappa,\alpha\right) \tag{17}$$

The corresponding first partial derivatives are:

$$\frac{\partial r_i}{\partial\alpha} = e^{\kappa\cos(\varphi_i-\mu)}e^{-\kappa} - 1 \tag{18}$$

$$\frac{\partial r_i}{\partial\kappa} = \left(\widehat{A}-\alpha\right)e^{\kappa\cos(\varphi_i-\mu)}e^{-\kappa}\left(1-\cos\left(\varphi_i-\mu\right)\right) \tag{19}$$

One of the crucial aspect in the GN-algorithm is the determination of the step-size $\lambda^n$. If the score-function is in fact quadratic w.r.t. to the parameter vector a step size of 1 would be the optimal solution leading to only one iteration necessary for the algorithm to converge. In all other cases the step size has to be chosen such that it leads to a further minimization of the score-function. For the paper at hand we used a simple search procedure: starting from $\lambda=1$ it halves the value of $\lambda$ until the value of the score-function is less than the value during the previous iteration. In other words the following condition has to be fullfilled for $\lambda^n$:

$$\epsilon\left(\boldsymbol{\theta}^n+\lambda^n\boldsymbol{\Delta\theta}^n\right) < \epsilon\left(\boldsymbol{\theta}^n\right) \tag{20}$$

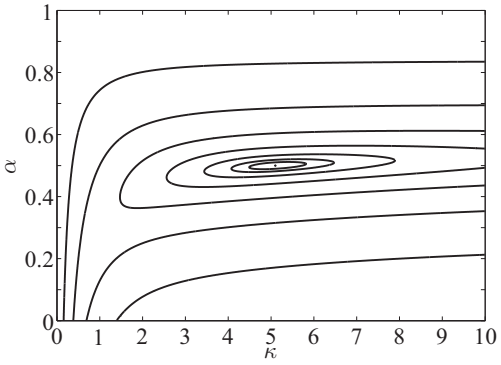


Fig. 1. Contour of score-function $\epsilon(\alpha, \kappa)$ of synthetic example ($\kappa = 5.1, \alpha = 0.5$), contour lines show the error values $[0, 0.01, 0.03, 0.1, 1.0, 3.1, 10]$

The search for the best value of $\lambda$ is utlimately stopped if the computational accuracy of the computer is reached ($\lambda$ being less than the computers accuracy). Global convergence is defined to be reached if the relative change of the parameters at a certain iteration is below a given threshold (we used $10^{-10}$ for this contribution). Fig 1 shows an example of the score-function $\epsilon(\alpha, \kappa)$ (Eqn. (12)) using synthetic input data. As you can see the score-function is not quadratic especially far away from the optimum value. For large values of $\kappa$ the shape of the score-function gets more and more flat which negatively influences the performance of the GN-algorithm or can even cause it to fail. However, if the estimation is started in the vicinity of the optimum we experienced a good performance of the GN-algorithm (small number of iterations). Therefore, we can conclude that the initialisation of the estimation is of highest importance. To find those initial values we implemented a grid-based search (brute-force) using a rather coarse grid for $\alpha$ and $\kappa$.

$$\alpha_{ini} = \left[\min_{\varphi}\left(A(\varphi)\right) : \Delta\alpha_{ini} : \overline{A}(\varphi)\right] \tag{21}$$

$$\kappa_{ini} = [0 : \Delta\kappa_{ini} : 30] \tag{22}$$

$$\Delta\alpha_{ini} = \frac{\overline{A}(\varphi) - \min_{\varphi}\left(A(\varphi)\right)}{10} \tag{23}$$

$$\Delta\kappa_{ini} = 3 \tag{24}$$

with $\overline{A}(\varphi)$ being the mean value of $A(\varphi)$. The maximum value of $\kappa_{ini}$ is chosen in accordance with the minimum width of the beamformer of the antenna arrays described in the following section [5].

## V. Measurement Data

In this section results are presented that are obtained from a MIMO-measurement campaign conducted in the city centre of Ilmenau, Germany. A detailed description of the campaign can be found in [8]. The analysis is limited to the receiver side and to the azimuth angle because of azimuthal angular resolution of the receiving array is highest for the given measurement

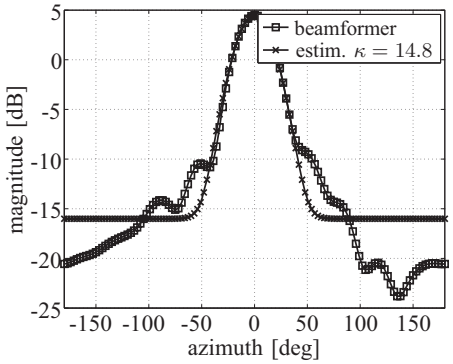


Fig. 2. Estimator applied to a single specular path as input data, the width of the beamformer cannot get smaller than this leading to an upper bound of $\kappa$ of 14.8

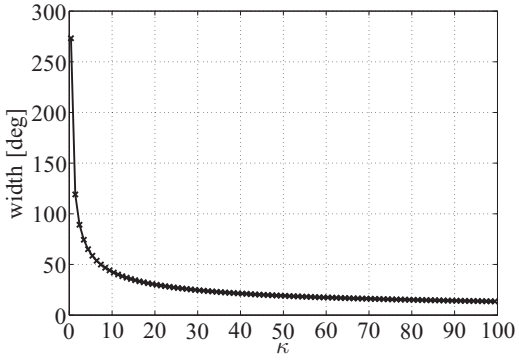


Fig. 3. 3dB-width of VMD depending on $\kappa$

setup. Furthermore, only the nine publicly available measurement files (as described in [8]) are analyzed. At the receiving side a Stacked-Polarimetric-Uniform-Circular-Array (SPUCA) having two rings with 12 dual-polarized patch antennas each was used. This array has an azimuthal angular resolution of $\approx 30°$. That means the width of the beamformer output is lower limited to $30°$ thus possing a lower bound on the width of the estimated VMD as well. Fig. 2 shows the beamformer output and the estimated VMD for the azimuth domain using a single specular path as input data. Fig. 3 shows the mapping of the parameter $\kappa$ of the VMD to the corresponding 3dB-width. Due to the minimal width of the beamformer any estimated $\kappa$ whose value is above 14.8 ($\kappa$ corresponding to the minimal width of the beamformer) should not be treated as a valid estimation result.

## VI. Results

### A. Power of specular paths vs. DMC

At first we want to take a look at the amount of power of the estimated DMC compared to the specular paths and the measurement noise. Fig 4 shows the Cumulative-distribution-function (CDF) of the ratio of the total power of the specular paths and the estimated DMC for the nine different files. The mean value of the power-ratio is between 7 and 11 dB

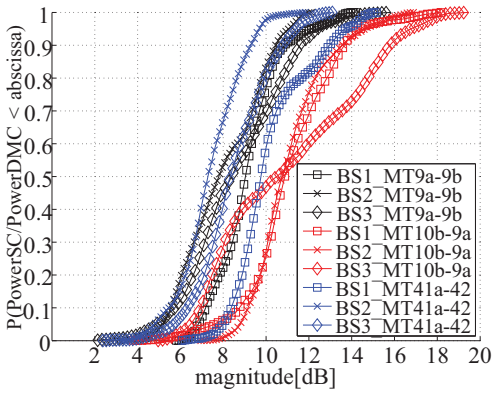


Fig. 4. CDF of power ratio of specular paths (SC) and DMC

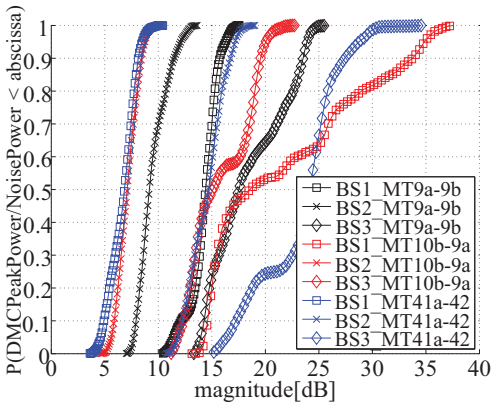


Fig. 5. CDF of dynamic range of estimated DMC w.r.t. noise power

indicating that the radio channel is nearly always dominated by the specular paths. This is a common result for urban-macrocell or in general outdoor measurements.

### *B. Signal-to-Noise-Ratio (SNR) of the DMC*

In order to achieves good estimates of the angular properties of the DMC the SNR of the DMC has to be high enough. We use the ratio between the DMC-Peakvalue $\alpha_1$ and the noise level $\alpha_0$ as an estimate of the SNR or the dynamic range (DR) of the DMC respectively. Fig 5 shows the CDF of that ratio. Note that the ratio of $\alpha_1$ and $\alpha_0$ is not the total SNR as it does not take into account the total power of the DMC but only the peak-power. It can be seen that the DR is rather low for the three files "BS1_MT41a-42","BS2_MT10b-9a" and "BS2_MT9a-9b". Therefore, these files will be excluded from further analysis. The next figures show the results of the estimation of the angular properties of the DMC. In order to avoid the inclusion of too much noise samples the data is pre-processed by applying a time-domain window that removes (zeroes out) all samples whose power is less than 6dB above the noise power.

### *C. Estimation results using beamformer output*

Before investigating the actual parameters of the VMD it is interesting to investigate the DR of the beamformer output without applying any estimation. This will already give a measure of how much the DMC is concentrated in the angular domain. The DR is computed as the ratio between the peak and the average value of the different beamformer outputs. In Fig. 6 the DRs are shown. It is apparent that the DR is in general really low; the 50% threshold is lower than 3dB. This is surprising as it indicates that there is no significant angular concentration in most of the cases. Since we limited the analysis to cases where the DMC has sufficient SNR this phenomenon should not be caused by the measurment noise. It is moreover an indication that the DMC appears to posses a uniformly shaped distribution in the angular domain. Similiar results are already obtained in [5]. However, one must not forget that these observation are based upon the beamformer output which is inherently dependent on the antenna arrays used. It is possible that the uniform shape of the beamfomer output is comprised of a larger number of overlapping e.g. VMDs whose width is too low for the beamformer to resolve. Furthermore, the presence of multiple strong (in terms of power) VMDs might lead to a low DR since the DR (as defined above) is only suitable to evaluate a single/unimodal VMD. However, based on our experience with the measurement data and the estimation results the former explanation (dominant UD) is more likely. In the following the results for the estimated VMD parameter $\kappa$ is presented. Based on the observations about the DR only data is considered having a DR higher than 3dB. Fig 7 shows the results for the $\varphi$- and $\vartheta$-polarization respectively. The rough shape of the curves especially in case of the $\varphi$-polarization can be explained by the limited amount of data due to the limitation of DR being higher than 3dB. The $\vartheta$-polarization gives better results since in general the DR is higher in this case (see Fig. 6b). From the figures we can conclude that the majority of that data leads then to an estimated VMD with angular width being bigger than the resolution of the array (see Fig. 3 and 2). Therefore, the estimated VMDs reflect the actual angular properties of the DMC. The cases were the estimated VMD width is smaller than the resolution of the array (which imposes an ultimate lower bound on the width) can be explained by estimation inaccuracies. As stated above the DR was limited to >3dB which is a somewhat arbitrary threshold and does not avoid estimation errors.

## VII. Conclusions

In this paper we have used an GN based algorithm to estimate the angular properties of the DMC in an urban-macrocell scenario. We found that the power of the estimated DMC is ca. 7-10dB below the power of the specular paths in this scenario. The most important finding is that in a lot of cases the DMC appears to be uniformly distributed or the DR of the beamformer output does not allow for an valid estimation of a concentrated VMD respectively. However, this does not mean that an angular model of the DMC is unnecessary. The results presented in this paper are only valid for the measurements conducted in Ilmenau, Germany. The

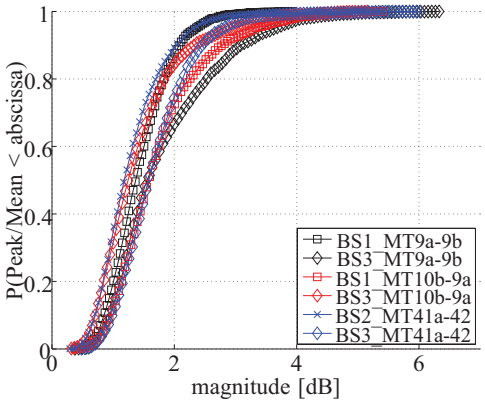


(a) CDF of dynamic of beamformer $\varphi$-polarization

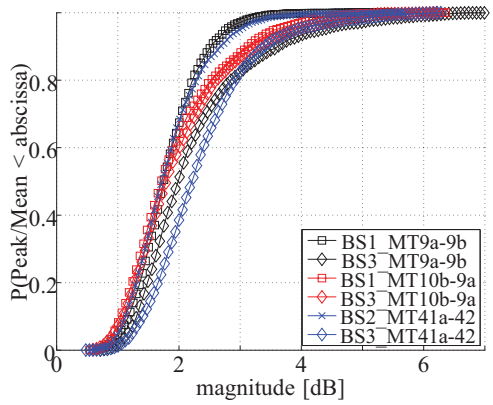


(b) CDF of dynamic of beamformer $\vartheta$-polarization

Fig. 6. CDF of the dynamic of the beamformer output as the ratio of peak and average value

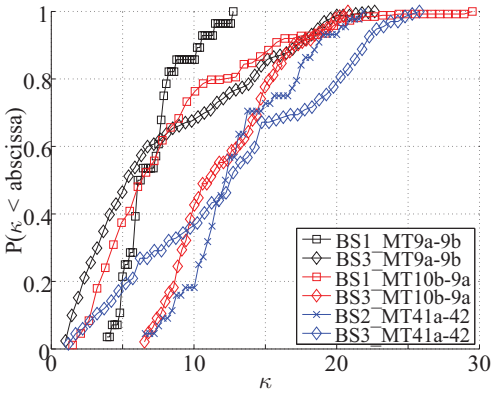


(a) CDF of estimated $\kappa$ for $\varphi$-polarization

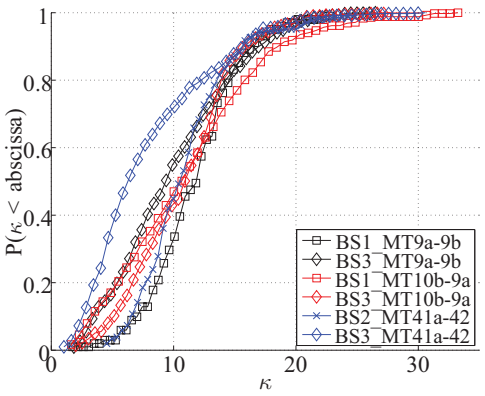


(b) CDF of estimated $\kappa$ for $\vartheta$-polarization

Fig. 7. CDF of the estimated values of $\kappa$, rough shape of $\varphi$-polarization is caused by limited number of samples due to limitation of data with DR higher than 3dB

estimator used in the paper is based on beamforming, thus, being highly dependent on the characteristics of the antenna arrays used. It is most likely that the results will differ in different scenarios and with different antenna arrays. Furthermore, the UD discussed here is not equivalent to the DMC-model having identity matrices for the receive and transmit covariance matrices (Eqn. (3)). If identity matrices are used it is assumed that there is no correlation between the different array elements. This is, however, not true since it ignores the correlation introduced by the array itself. Therefore, it can be concluded that even if the DMC appears to be uniformly distributed in the angular domain the model of the DMC should still contain the correlation properties of the antenna array by using realistic covariance matrices instead of identity matrices.

## ACKNOWLEDGMENT

This work has been supported by the UMIC Research Center, RWTH Aachen University.

## REFERENCES

[1] Richter A., "*On the Estimation of Radio Channel Parameters: Models and Algorithms (RIMAX)*," Doctoral thesis, Technische Universität Ilmenau, Germany, May 2005.

[2] Ribeiro C.B., Richter A., and Koivunen V., "Joint Angular- and Delay-Domain MIMO Propagation Parameter Estimation Using Approximate ML Method," *IEEE TRANSACTIONS ON SIGNAL PROCESSING*, vol. 55, pp. 4775–4790, October 2007.

[3] J. Salmi, J. Poutanen, K. Haneda, A. Richter, V.-M. Kolmonen, P. Vainikainen, and A. F. Molisch, "Incorporating diffuse scattering in geometry-based stochastic mimo channel models," in *Antennas and Propagation (EuCAP), 2010 Proceedings of the Fourth European Conference on*, 2010, pp. 1 –5.

[4] Francois Quitin, Claude Oestges, Francois Horlin, and Philippe De Doncker, "Diffuse multipath component characterization for indoor mimo channels," in *Antennas and Propagation (EuCAP), 2010 Proceedings of the Fourth European Conference on*, 2010, pp. 1 –5.

[5] Käske M., Landmann M., and Thomä R.S., "Modelling and Synthesis of Dense Multipath Propagation Components in the Angular Domain," in *3rd European Conference on Antennas and Propagation*, March 2009.

[6] Landmann M., "*Limitations of Experimental Channel Characterisation*," Doctoral thesis, Technische Universität Ilmenau, Germany, March 2008, ISBN (E-Book): 978-3-640-20944-6, available to download at http://www.grin.com.

[7] Cattermole K.W. and O'Reilly J.J, *Optimierung in der Nachrichtentechnik*, Number 3-527-26614-3. VCH, 1990.

[8] Schneider C., Sommerkorn G., Narandzic M., Käske M., Hong A., Algeier V., Kotterman W., Thomä R. S., and Jandura C., "Multi-user mimo channel reference data for channel modelling and system evaluation from measurements," in *International IEEE Workshop on Smart Antennas (WSA 2009)*, Berlin, Germany, February 2009.